Stochastic explanation of speckle contrast detection in ultrasound-modulated optical tomography

Roger Zemp, Sava Sakadžić, and Lihong V. Wang*
Optical Imaging Laboratory, Department of Biomedical Engineering, Texas A&M University, College Station, Texas 77843-3120, USA
(Received 10 February 2006; published 27 June 2006)

Ultrasound-modulated optical tomography is an imaging technique that detects ultrasonically tagged light in optically turbid media to obtain images with optical contrast and ultrasonic spatial resolution. A CCD-camera-based speckle contrast detection scheme has been introduced previously to detect modulated light emerging from the ultrasonic sample volume. Differences in speckle contrast were experimentally observed when ultrasound was applied compared to when it was not. In this paper we provide an analytic explanation for this phenomenon and connect speckle statistics with ultrasonic field parameters. The theory predicts that speckle contrast changes linearly with applied acoustic intensity. This prediction is experimentally validated for both 1 and 3.5 MHz ultrasound. Signal dependence on ultrasound frequency is discussed.

DOI: 10.1103/PhysRevE.73.061920 PACS number(s): 87.64.Cc, 87.57.−s, 85.60.Gz, 87.63.Df

I. INTRODUCTION

Optical imaging of soft tissue in living subjects with high spatial resolution and significant penetration depths remains a challenge due to multiplyscattered light. Ultrasoundmodulated optical tomography (UOT), also referred to as acousto-optical tomography, aims to locally probe tissue optical properties by modulating the optical field within a spatially confined, focused region of ultrasound. By sweeping the ultrasonic sample volume in tissue, images are formed representative of the amount of modulated light emerging from the ultrasonic sample volume, hence the images provide information about optical properties such as absorption and scattering. Theoretical contributions explaining the mechanisms of the ultrasonic modulation of light in optically scattering media have been offered by Leutz and Maret [1], Mahan [2], Lev [3,4], Wang [5,6], Sakadžić and Wang [7,8], among others. Various detection systems have been devised to detect the modulated component of light emerging from tissue including single square-law detectors [9], CCD cameras [10–13], Fabry-Perot interferometers [14], and photorefractive detection schemes [15,16].

This paper is concerned with speckle contrast detection, introduced for UOT in Ref. [11]. A phenomenological explanation for this scheme was given in Ref. [11], however, no connection was made to acoustic parameters. We provide a more rigorous analysis based on the speckle statistics and probabilistic models of ultrasound-modulated light propagation introduced in Refs. [5–8]. The model provides important justification for the detection scheme, and offers insights into ultrasonic parameter selection. Experiments validate predicted linear relationships between speckle contrast and acoustic intensity.

II. THEORY

A. Statistical model of speckle contrast for UOT

We wish to establish a theoretical framework for modeling speckle contrast as a function of acoustic and optical parameters. Consider the propagation of temporally coherent light through a homogeneous optically scattering medium with discrete optical scatterers insonified by a monochromatic ultrasound plane wave. The time-intensity profile $I_p(t)$ of one speckle spot (coherence area) matched to one detector element can be given as the intensity of electric field due to a sum of many scattered wave components. Neglecting polarization for simplicity, the electric field on the detector element p of the detector array may be written as follows:

$$E_p(t) = \left(\sum_{i=1}^{N_p} E_i(t) \right), \tag{1}$$

and the intensity as

$$I_p(t) = |E_p(t)|^2 = \left(\sum_{j=1}^{N_p} \sum_{i=1}^{N_p} E_i(t) E_j^*(t) \right), \tag{2}$$

where the expressions are evaluated for a single realization of a scatterer distribution Ξ and $E_i(t)$ is the complex electric field contribution of the ith partial wave due to a given scattered light path. N_p is the number of partial waves originating from N_p photon paths.

1. First order statistics

To compute the speckle contrast we require the mean and variance of the speckle intensity distribution from one CCD exposure. The time-averaged intensity of one speckle spot is given as $\overline{I_p} = \langle I_p(t) \rangle_t$. In this paper we assume light-integration times T are much longer than optical and ultrasonic periods such that effectively $\langle I_p(t) \rangle_t = \lim_{T \to \infty} \frac{1}{T} \int_0^T I_p(t) dt$. The mean intensity averaged over pixels p of the CCD is given as follows:

$$\langle \overline{I_p} \rangle_p \approx \langle \overline{I_p} \rangle_\Xi = \left\langle \left(\sum_{i=1}^{N_p} \sum_{j=1}^{N_p} E_i(t) E_j^*(t) \right) \right\rangle_{\Xi,t}. \tag{3}$$

Here the middle equality follows from an assumption of spatial ergodicity [17], that is, we assume that the first and second-order speckle statistics are not spatially varying.

We also assume that the photon mean free path is much longer than the optical wavelength (weak scattering approxi-

*Email address: Lwang@tamu.edu

mation) and the acoustic particle displacements are much less than the optical wavelength.

With these conditions in mind, Eq. (3) is evaluated as follows:

$$\langle \overline{I_p} \rangle_p \approx G_1(0) = I_0, \tag{4}$$

where I_0 is the mean optical intensity. Here

$$G_1(\tau) = \langle \Gamma_1(t,\tau) \rangle_t \tag{5}$$

is the time average of the temporal field autocorrelation function [5,7]

$$\begin{aligned}\Gamma_1(t,\tau) &= \langle E_p(t) E_p^*(t+\tau) \rangle_\Xi \\ &= \sum_{i=1}^{N_p} \sum_{j=1}^{N_p} \langle E_i(t) E_j^*(t+\tau) \rangle_\Xi \\ &= \sum_{i=1}^{N_p} \langle E_i(t) E_i^*(t+\tau) \rangle_\Xi \\ &= \int_0^\infty p(s) \langle E_s(t) E_s^*(t+\tau) \rangle_H ds. \end{aligned} \tag{6}$$

In Eq. (6) we follow the diffusing-wave spectroscopy approach [18,19], where it is assumed that in the weak scattering approximation the correlation between different random paths vanishes and only the photons traveling along the same physical path (meaning a given sequence of scatterers) produce a nonzero effect. $E_s(t)$ is the electric field from paths of length s and $p(s)$ is the probability density function of s. H is the space of all possible realizations of paths of path length s (discussed more precisely in Refs. [7,8]). Because s is related to photon propagation times, in the diffusion regime, $p(s)$ can be modeled by time-resolved diffusion-theoretic approaches [20]. Our assumptions of spatial ergodicity rely on the fact that the CCD detector is sufficiently far from the sample that the modulated diffuse light produces a fairly uniform speckle field over the CCD surface. In Eq. (6) we neglect Brownian motion or assume that the CCD integration time is sufficiently brief so as to ignore Brownian motion induced speckle decorrelation.

2. Second order statistics

Here we want to compute the variance of the speckle pattern on the CCD surface. As a first step in computing the speckle variance, we rely on spatial ergodicity to compute the second-order moment of intensity:

$$\begin{aligned}\langle \overline{I_p}^2 \rangle_p \approx \langle \overline{I_p}^2 \rangle_\Xi &= \langle \langle E_p(t) E_p^*(t) \rangle_t \langle E_p(t') E_p^*(t') \rangle_{t'} \rangle_\Xi \\ &= \langle \langle E_p(t) E_p^*(t) E_p(t') E_p^*(t') \rangle_\Xi \rangle_{t,t'}. \end{aligned} \tag{7}$$

When we make the substitution $t' = t + \tau$, this is recognized as $\langle G_2(\tau) \rangle_\tau$, where $G_2(\tau) = \langle I_p(t) I_p(t+\tau) \rangle_{\Xi,t}$ is the time-averaged temporal intensity autocorrelation function.

Now from Eq. (1) we note that the complex electric field E_p is composed of a large number of statistically independent zero-mean random processes, E_i. Hence, by virtue of the Central Limit Theorem [17], $E_p(t)$ is well modeled by a zero-mean complex normal process with an approximately uniformly distributed phase. Normality allows us to write the fourth order moment of the electric field as follows [21]:

$$\begin{aligned}&\langle E_p(t) E_p^*(t) E_p(t+\tau) E_p^*(t+\tau) \rangle_\Xi \\ &= \langle E_p(t) E_p^*(t) \rangle_\Xi \langle E_p(t+\tau) E_p^*(t+\tau) \rangle_\Xi \\ &\quad + \langle E_p(t) E_p(t+\tau) \rangle_\Xi \langle E_p^*(t) E_p^*(t+\tau) \rangle_\Xi \\ &\quad + \langle E_p(t) E_p^*(t+\tau) \rangle_\Xi \langle E_p^*(t) E_p(t+\tau) \rangle_\Xi, \end{aligned} \tag{8}$$

thus breaking the expectation over scatterer realizations Ξ into a product of second order moment contributions. Noting that the second term on the right-hand side of Eq. (8) vanishes due to ensemble averaging over a uniformly distributed phase and using Eq. (6), the second moment of speckle intensity, Eq. (7), can be written as follows:

$$\langle G_2(\tau) \rangle_\tau = G_1^2(0) + \langle |\Gamma_1(t,\tau)|^2 \rangle_{t,\tau} \tag{9}$$

and the variance is then simply

$$\sigma^2 = \langle |\Gamma_1(t,\tau)|^2 \rangle_{t,\tau}. \tag{10}$$

At this point we need to express the autocorrelation function (6) as follows:

$$\Gamma_1(t,\tau) = I_0 \int_0^\infty p(s) \langle \exp(-i \Delta\varphi_s(t,\tau)) \rangle_H ds, \tag{11}$$

where $\Delta\varphi(t,\tau)$ is the difference of the accumulated phase due to the ultrasound-modulation mechanisms at two time moments along the same path, which we assume is small for small ultrasonic pressures, and for further conditions discussed in Ref. [8]. Then we may use a Taylor expansion. First-order terms average to zero, and terms higher than second order are neglected. Consequently, to the second order,

$$\langle |\Gamma_1(t,\tau)|^2 \rangle_{t,\tau} = I_0^2 \left(1 - \int_0^\infty p(s) \langle \Delta\varphi_s^2(t,\tau) \rangle_{H,t,\tau} ds \right). \tag{12}$$

Now our problem reduces to evaluating $\langle \Delta\varphi_s^2(t,\tau) \rangle_{H,t,\tau}$. The difference of the accumulated phase

$$\Delta\varphi_s(t,\tau) = \Delta\varphi_{s,n}(t,\tau) + \Delta\varphi_{s,d}(t,\tau), \tag{13}$$

is due to two physical mechanisms: ultrasound-induced optical scatterer displacement and ultrasound-induced changes in the optical refractive index of the medium, represented by the first and second terms on the right-hand side of Eq. (13), respectively.

The evaluation of the second-order moment of $\Delta\varphi_s$:

$$\langle \Delta\varphi_s^2(t,\tau) \rangle_{H,t} = \langle \Delta\varphi_{s,n}^2 \rangle_{H,t} + \langle \Delta\varphi_{s,d}^2 \rangle_{H,t} + \langle 2 \Delta\varphi_{s,n} \Delta\varphi_{s,d} \rangle_{H,t} \tag{14}$$

was calculated in Eq. (29) of Ref. [8], assuming isotropic scattering, where $\langle \Delta\varphi_{s,n}^2 \rangle_{H,t}$, $\langle \Delta\varphi_{s,d}^2 \rangle_{H,t}$, and $\langle \Delta\varphi_{s,n} \Delta\varphi_{s,d} \rangle_{H,t}$ are the auto and cross correlations of accumulated optical phase differences due to ultrasound-induced optical refractive index changes and time-varying optical scatterer displacements. Averaging over τ gives our desired results:

$$\langle \Delta\varphi^2(t,\tau)\rangle_{H,t,\tau} = \frac{1}{2}(C_n + C_d + C_{n,d}), \tag{15}$$

where C_n, C_d, and $C_{n,d}$ are given by Eq. (30) of Ref. [8]:

$$C_n = \Lambda^2 \frac{\eta^2}{k_a^2}(k_a l)^2 \left[\left(\frac{s}{l} + 1 \right) \frac{G}{1-G} - \frac{G^2(1-G^{s/l+1})}{(1-G)^2} \right],$$

$$C_d = \Lambda^2 \frac{S^2}{k_a^2} \left[\frac{s}{3l} - \frac{1-G^{s/l-1}}{(k_a l)^2} \right],$$

$$C_{n,d} = \Lambda^2 \frac{2\eta S \cos(\phi)}{k_a^2} \left[-\frac{s}{l} + \frac{G(1-G^{s/l})}{1-G} \right]. \tag{16}$$

Here $\Lambda = 2n_0 k_0 P_0/(\rho v_a^2)$, where n_0 is the optical index of refraction, $k_0 = 2\pi/\lambda_0$ is the magnitude of the optical wave vector, λ_0 is the optical wavelength in vacuum, P_0 is the ultrasound pressure amplitude, ρ is the mass density of the medium, and v_a is the ultrasound velocity. k_a is the ultrasonic wave vector magnitude, and η is the elasto-optic coefficient, approximately equal to 0.32 in water at standard conditions. S and ϕ are the relative displacement amplitude and phase lag between the optical scatterers and the fluid motion, approximated as ≈ 1 and ≈ 0, respectively, in our subsequent analysis, and discussed further in Ref. [8].

In Eq. (16), $G = (k_a l)^{-1} \arctan(k_a l)$, where l is the isotropic mean-free path. Anisotropic scattering can be considered by exploiting an approximate similarity relation and replacing l with the transport mean-free path $l_{tr} = l/(1-g)$ (where g is the scattering anisotropy factor) in the above equations.

3. Contrast of speckles

Speckle contrast is defined

$$C = \frac{\sigma}{\langle \bar{I}_s \rangle_p}. \tag{17}$$

Inserting calculated values for mean and standard deviation of speckle intensity, we have

$$C = \frac{\sqrt{\langle |\Gamma_1(t,\tau)|^2 \rangle_{t,\tau}}}{G_1^2(0)} \approx 1 - \frac{1}{2}\int_0^\infty p(s)\langle \Delta\varphi_s^2(t,\tau)\rangle_{H,t,\tau} ds, \tag{18}$$

where the last expression keeps only terms to first order in $\langle \Delta\varphi_s^2(t,\tau)\rangle_{H,t,\tau}$, appropriate for small ultrasonic pressures. The difference in speckle contrast ΔC between ultrasound off and ultrasound on states is given by the magnitude of the second term in the right-hand side of Eq. (18), evaluated as follows:

$$\Delta C = \frac{1}{2}\int_0^\infty p(s)(C_n + C_d + C_{n,d}) ds. \tag{19}$$

Since all the C terms of Eq. (16) are proportional to P_0^2 we note that ΔC is proportional to acoustic intensity. In this article we validate this linear relationship between speckle contrast and acoustic intensity with experimental data. Although the theory is limited in its scope it provides greater intuition and analytical motivation behind speckle contrast detection and acoustic and optical parameter selection.

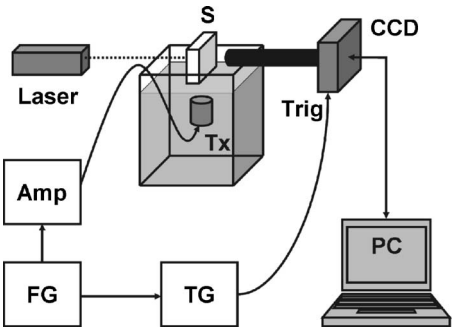

FIG. 1. Experimental setup. *S*, sample; CCD, CCD camera; AMP, RF amplifier; FG, function generator; TG, trigger generator; Tx, ultrasound transducer.

4. High ultrasound frequencies

Here we consider ultrasound frequencies f_a high enough that $k_a l_{tr}$ is larger than, preferably much larger than 1. In this case G tends to $\pi/(2k_a l_{tr})$. Also, since our framework is derived for the diffusion regime, we should consider optical scattering paths much longer than the transport mean-free path. In this case $C_n + C_d + C_{n,d} \approx C_n$ which is approximately $\Lambda^2 \frac{\eta^2}{k_a^2}(k_a l_{tr})^2 G \frac{s}{l_{tr}}$, and the change in speckle contrast between ultrasound on and ultrasound off states, ΔC, is given as follows:

$$\Delta C \approx \frac{\bar{s}}{4}\left(n_0 k_0 \frac{P_0}{\rho v_a^2} \right)^2 \eta^2 \frac{v_a}{f_a}. \tag{20}$$

The term $\bar{s} \equiv \int_0^\infty s p(s) ds$ reflects the mean path length for a given light-propagation geometry. For example we might consider transmission and reflection of light through a slab as considered analytically in the diffusion regime by Ref. [20]. Then $\int_0^\infty s p_T(s) ds$ and $\int_0^\infty s p_R(s) ds$ represent mean transmission and reflection path lengths, respectively, for given positions of source and detector.

The more general expression, Eq. (19), more accurately accounts for correlations between ultrasound-induced optical phase increments along the photon path, although it is more difficult to compute. In particular it accounts for correlations between ultrasound-induced optical phase increments when $k_a l_{tr}$ is not $\gg 1$.

III. EXPERIMENT

Our experimental setup is illustrated in Fig. 1 and includes a laser source, ultrasound transducer, imaging sample, CCD camera, and timing synchronization electronics. To acquire one point of an image we apply ultrasonic bursts while using a CCD camera to detect modulated light originating from the ultrasonic sample volume. We used a frequency-doubled Nd:YAG laser due to its stability and long coherence length (Coherent, Verdi; 532-nm wavelengths). We used a 1-MHz transducer (Ultran VHP100-1-138) with 38-mm focal length and a 3.5-MHz transducer (Panametrics V380)

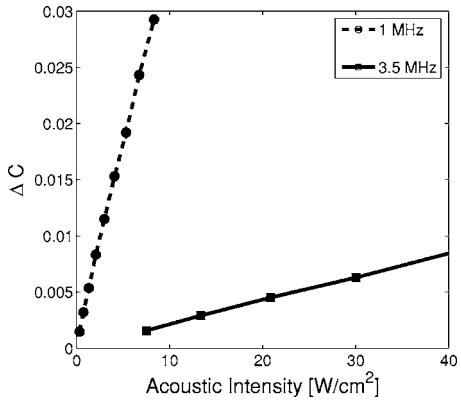

FIG. 2. Plot of the change in speckle contrast ΔC (between ultrasound off- and on-states) for 1- and 3.5-MHz transducers versus acoustic intensity I_{spta}.

with 49-mm focal length. Both transducers had a 25 mm diameter active aperture. The laser beam was aligned in free space to pass through the ultrasonic focus such that the light and ultrasound directions were perpendicular to each other.

Speckle patterns emerging from the sample were captured by a digital CCD camera (Basler, A312f; 12-bit, 640×480) such that the average speckle spot size was matched to the CCD pixel size. A light tube with the appropriate aspect ratio was used to ensure this matching. A function generator (Agilent, 33250A) synthesized 2 ms bursts that were subsequently amplified by an RF amplifier (ENI, Inc., 325LA) to drive the ultrasound transducer. A low 1-Hz duty cycle was used to prevent damage to the transducer. Burst initiation triggered a pulse-delay generator (Stanford Research, DG535) that produced two CCD trigger pulses for each burst. One image was captured with the ultrasound on while the subsequent image was acquired with ultrasound off. Capturing on-off pairs allowed considerable robustness to slow speckle contrast drift due to environmental instabilities. For our sample we used a homogeneous 10% gelatin, 10% cornstarch phantom in a 2-cm thick slab geometry with reduced scattering coefficient $\mu_s'=9.2\,\mathrm{cm}^{-1}$ as measured by the oblique-incidence diffuse reflectance technique [22].

Here we experimentally investigate the theoretical prediction that laser speckle contrast decreases linearly with acoustic intensity. We do this by measuring speckle contrast with both 1-MHz and 3.5-MHz transducers. Pressures were measured in deionized water at room temperature with a broadband needle hydrophone and are accurate to ±10%. Rather than plot the decrease in speckle contrast, in Fig. 2 we plot the magnitude of the difference in speckle contrast, ΔC, between ultrasound off and ultrasound on as a function of time-averaged acoustic intensity. Fifty pairs of on-off speckle contrast measurements were used to estimate each data point and error bars are smaller than data marker sizes. Intensity is defined as $P_0^2/(2\rho v_a)$ where P_0 is the peak acoustic pressure, ρ is the mass density of the sample, and v_a is the speed of sound. This is often referred to as I_{spta}, the spatial peak time-averaged intensity.

IV. DISCUSSION

The trend in Fig. 2 is linear for both 1- and 3.5-MHz transducers as evidenced by the high linear correlation coefficients 0.9995 and 0.9978, respectively. These curves validate the theoretical prediction of linearity of signal with acoustic intensity, even though the theoretical model did not account for spatially varying acoustic fields.

It should be noted that the 1 MHz transducer offers considerably more signal than the 3.5 MHz transducer. It is noteworthy to comment on the frequency dependence of ΔC. The ratio of slopes between 1 and 3.5 MHz in Fig. 2 is approximately 18:1. Let us assume that we may use Eq. (20) as a rough estimate to compute an expected slope ratio to compare with the experiment. In doing so, let us approximate the acoustic field as plane-wave homogeneous over a bounded volume representative of the ultrasonic focal zone, and that this is the principal light-ultrasound interaction region. For 1 MHz, the mean photon path length $\bar{s}$ should be greater than the focal beam width of 2.3 mm and for 3.5 MHz $\bar{s}$ is close to the ultrasound beam focal width of 0.85 mm. In making estimates of the predicted slope ratios, we should note that the assumptions needed to make the theory analytically tractable do not closely match the experimental conditions. In particular: (i) the focal widths are likely too small to accurately use the diffusion approximation for light transport across the light-ultrasound interaction region: (ii) the acoustic field is spatially inhomogeneous rather than a plane wave: (iii) $k_a l_{tr}$ for 1 MHz is not much larger than 1 thus reducing the accuracy of Eq. (20): (iv) optical index of refraction changes due to pressures greater than 10^5 Pa may be large enough to bend photon paths in a way not presently accounted for by theory: (v) the theory does not account for polarization, Brownian motion, or imperfect temporal coherence of the laser source, effects that may tend to blur speckle contrast over the CCD exposure period. Indeed we note that the maximum ultrasound-off speckle contrast C_{max} experimentally observed is $\sim$0.3 rather than 1.

Another key point is that the amount of unmodulated light passing around the acoustic beam will influence the observed change in speckle contrast between ultrasound on- and off-states. Equations for ΔC such as Eq. (20) may be modified to include a multiplicative factor ζ which is representative of the fraction of light passing through the acoustic sample volume (see endnote [24]). In our situation, the fraction of light passing through the beam focal region is estimated as $\zeta_{1MHz}\sim0.3$ and $\zeta_{1MHz}\sim0.1$ [25].

Accounting for ζ, Eq. (20) predicts that the slope ratio should be $\sim$28:1. This very rough estimate differs from the measured slope ratio by approximately 50%. Using $C_{max}=0.3$, the absolute values of the slopes for 1 and 3.5 MHz are estimated within an order of magnitude of the measured values of $0.0037\,\mathrm{cm}^2/\mathrm{W}$ and $0.0002\,\mathrm{cm}^2/\mathrm{W}$, respectively. Although the experimental conditions do not closely match the conditions presently required to make the theory analytically tractable, the main point of the experimental results is to demonstrate the predicted linearity of ΔC with acoustic intensity, and to show that there is substantially more modulated light with low frequencies, compared with higher frequencies. Future work should account for modulated light transport through spatially varying acoustic fields, as well as modulated light transport across subdiffusion-regime sample volumes. Progress is being made to this end [23].

V. CONCLUSIONS

We have presented a stochastic model of speckle statistics in ultrasound-modulated optical tomography for plane-wave ultrasound and low acoustic intensities. The model predicts that speckle contrast will change linearly with acoustic intensity—a prediction validated experimentally. Significantly more modulated light is detected using 1-MHz ultrasound compared with 3.5-MHz ultrasound for the same acoustic intensity. The greater signal is attributed to a larger ultrasonic sample volume, larger ultrasound-induced particle displacement, and enhanced optical field modulation due to index-of-refraction mechanisms. The model suggests that the change in speckle contrast is proportional to the intensity of modulated light. The present model breaks down at high acoustic powers where substantial phase accumulation is expected. Future work should incorporate spatially varying acoustic fields, and optical heterogeneities.

ACKNOWLEDGMENTS

We gratefully acknowledge funding from the National Institutes of Health, R33 CA 094267.

[1] W. Leutz and G. Maret, Physica B **204**, 14 (1995).
[2] G. D. Mahan, W. E. Engler, J. J. Tiemann, and E. G. Uzgiris, Proc. Natl. Acad. Sci. U.S.A. **95**, 14015 (1998).
[3] A. Lev and B. G. Sfez, Opt. Lett. **27**, 473 (2002).
[4] A. Lev and B. Sfez, J. Opt. Soc. Am. A **20**, 2347 (2003).
[5] L. H. Wang, Phys. Rev. Lett. **87**, 043903 (2001).
[6] L. H. Wang, Opt. Lett. **26**, 11911193 (2001).
[7] S. Sakadžić and L. H. Wang, Phys. Rev. E **66**, 026603 (2002).
[8] S. Sakadžić and L. H. Wang, Phys. Rev. E **72**, 036620 (2005).
[9] L. H. Wang, S. L. Jacques, and X. Zhao, Opt. Lett. **20**, 629 (1995).
[10] S. Leveque, A. C. Boccara, M. Lebec, and H. Saint-Jalmes, Opt. Lett. **24**, 181 (1999).
[11] J. Li, G. Ku, and L. H. Wang, Appl. Opt. **41**, 6030 (2005).
[12] M. Kempe, M. Larionov, D. Zaslavsky, and A. Z. Genack, J. Opt. Soc. Am. **14**, 1151 (1997).
[13] J. Li and L. H. Wang, Appl. Opt. **41**, 2079 (2002).
[14] S. Sakadžić and L. H. Wang, Opt. Lett. **29**, 2770 (2004).
[15] F. Ramaz, B. C. Forget, M. Atlan, and A. C. Boccara, Opt. Express **12**, 5469 (2004).
[16] T. W. Murray, L. Sui, G. Maguluri, R. A. Roy, A. Nieva, F. Blonigen, and C. A. DiMarzio, Opt. Lett. **29**, 2509 (2004).
[17] A. Papoulis and S. U. Pillai, *Probability, Random Variables and Stochastic Processes*, 4th ed. (McGraw-Hill, New York, 2002).
[18] G. Maret and P. E. Wolf, Z. Phys. B **65**, 409 (1987).
[19] D. J. Pine, D. A. Weitz, P. M. Chaikin, and E. Herbolzheimer, Phys. Rev. Lett. **60**, 1134 (1988).
[20] M. S. Patterson, B. Chance, and B. C. Willson, Appl. Opt. **28**, 2331 (1989).
[21] D. Middleton, *An Introduction to Statistical Communication Theory* (Penninsula Publishing, Los Altos, CA, 1987).
[22] G. Marquez and L. H. Wang, Opt. Express **1**, 454 (1997).
[23] S. Sakadžić and L. H. Wang, Phy. Rev. Lett. (to be published).
[24] This is justified by modifying Eq. (11) as $\Gamma_1(t,\tau)=I_0\{(1-\zeta)+\zeta\int_0^\infty p(s)\langle\exp(-i\Delta\varphi_s(t,\tau))\rangle_H ds\}$ where ζ represents the fraction of light passing through the acoustic sample volume and $1-\zeta$ is the fraction of light passing around the acoustic sample volume. Continuing the derivations produces a modified Eq. (18) given as $\Delta C=1-\frac{1}{2}\zeta\int_0^\infty p(s)\langle\Delta\varphi_s^2(t,\tau)\rangle_{H,t,\tau}ds$.
[25] We assumed a 10 mm diffuse light pattern at the focal zone depth of 10 mm below the phantom, and estimate the area of the beam waist in this zone as a fraction of the total illumination area. For example, for 1 MHz, we estimate $\zeta=2.3$ mm $\times 10$ mm$/[\pi(5\text{ mm})^2]$.